How to cite: Angew. Chem. Int. Ed. 2024, e202316698
doi.org/10.1002/anie.202316698

Solar Cells

Binary All-polymer Solar Cells with a Perhalogenated-Thiophene-Based Solid Additive Surpass 18 % Efficiency

Wanying Feng., Tianqi Chen, Yulu Li, Tainan Duan, Xue Jiang, Cheng Zhong, Yunxin Zhang, Jifa Yu, Guanghao Lu, Xiangjian Wan, Bin Kan,* and Yongsheng Chen**

Abstract: Morphological control of all-polymer blends is quintessential yet challenging in fabricating high-performance organic solar cells. Recently, solid additives (SAs) have been approved to be capable in tuning the morphology of polymer: small-molecule blends improving the performance and stability of devices. Herein, three perhalogenated thiophenes, which are 3,4-dibromo-2,5-diiodothiophene (SA-T1), 2,5-dibromo-3,4-diiodothiophene (SA-T2), and 2,3-dibromo-4,5-diiodothiophene (SA-T3), were adopted as SAs to optimize the performance of all-polymer organic solar cells (APSCs). For the blend of PM6 and PY-IT, benefitting from the intermolecular interactions between perhalogenated thiophenes and polymers, the molecular packing properties could be finely regulated after introducing these SAs. In situ UV/Vis measurement revealed that these SAs could assist morphological character evolution in the all-polymer blend, leading to their optimal morphologies. Compared to the as-cast device of PM6:PY-IT, all SA-treated binary devices displayed enhanced power conversion efficiencies of 17.4–18.3 % with obviously elevated short-circuit current densities and fill factors. To our knowledge, the PCE of 18.3 % for SA-T1-treated binary ranks the highest among all binary APSCs to date. Meanwhile, the universality of SA-T1 in other all-polymer blends is demonstrated with unanimously improved device performance. This work provide a new pathway in realizing high-performance APSCs.

Introduction

All-polymer solar cells (APSCs) comprising polymer electron donor and acceptor materials have the potential to be used in the construction of ultra-flexible, intrinsically stretchable, and stable devices.[1] Notably, polymerized small-molecular acceptors (PSMAs) can easily overcome the limitations of conventional donor–acceptor (D–A) polymer acceptors and inherit the merits of both small-molecular acceptors (SMAs) and polymers (broad and effective light absorption, tunable electronic behaviors, excellent film-forming characters, *etc.*).[2] Recently, based on the development of Y6 molecules and new polymer donors, the performance of APSCs was improved to over 18 % efficiency.[3] Despite these achievements, considerable efforts are required for improving the performance of APSCs to meet the performance of polymer-SMA based devices as well as the requirements for their practical applications.

The realization of such goals requires a highly-efficient photoelectrical conversion process, which is mainly determined by the morphologies of the active layers.[4] However, owing to similarities in the chemical structures as well as the large molecular size of polymer donors and acceptors, the regulation of the morphology of all-polymer blends is challenging.[5] As summarized in Table S1, 1-chloronaphthalene (CN) is the most commonly solvent additive used in the tuning of morphologies of highly efficient all-polymer blends.[6] However, the usage of solvent additives is hindered to some extent because of the difficulty in being completely removed during the film-forming process, which induces some inferior effects on the long-term stability of devices and large-area manufacturing.[7] Thus, the development of highly volatile solid additives is mandatory.

[*] W. Feng., T. Chen, Y. Zhang, Prof. B. Kan
School of Materials Science and Engineering, National Institute for Advanced Materials, Nankai University
300350 Tianjin (China)
E-mail: kanbin04@nankai.edu.cn

W. Feng., Prof. X. Wan, Prof. Y. Chen
State Key Laboratory and Institute of Elemento-Organic Chemistry, Frontiers Science Center for New Organic Matter, The Centre of Nanoscale Science and Technology and Key Laboratory of Functional Polymer Materials, Renewable Energy Conversion and Storage Center (RECAST), College of Chemistry, Nankai University
300071 Tianjin (China)
E-mail: yschen99@nankai.edu.cn

Y. Li, Dr. T. Duan, X. Jiang
Chongqing Institute of Green and Intelligent Technology, Chongqing School, University of Chinese Academy of Sciences (UCAS Chongqing), Chinese Academy of Sciences
400714 Chongqing (China)
E-mail: tnduan@cigit.ac.cn

Dr. C. Zhong
Hubei Key Laboratory on Organic and Polymeric Opto-electronic Materials, College of Chemistry and Molecular Sciences, Wuhan University
430072 Wuhan (China)

J. Yu, Prof. G. Lu
Institute of Science and Technology, Xi'an Jiaotong University
710054 Xi'an (China)

Hou et al. (2019) pioneered a series of solid additives (SAs), which play a vital role in enhancing the molecular packings and crystallinity of electron donor/acceptor (D/A) blends, and realized more ordered π-π stackings, an improved charge transport, an enhanced performance, and long-term stability of devices.[8] Subsequently, numerous SAs were developed to achieve power conversion efficiency (PCE) of more than 19% for binary or ternary devices.[9] However, to our knowledge, very few SAs have been successfully applied to tune morphologies of all-polymer blends and thus realize high-performance APSCs (Table S1). Recently, Sun et al. proposed a rare successful case for obtaining over 17% PCE for PM6:PY-DT-based APSCs, where 2-methoxynaphthalene (2-MN) is used as the SA.[10] Most recently, Liu et al. adopted the 1,4-diiodobenzene (DIB) to tune morphologies of PM6:PY-IT and obtained a PCE of over 18% by combining thermal and solvent annealing as well as optimizing the hole transporting layer.[11] Most of the reported SAs are derived from halogenated benzene units, such as DIB,[12] 1,3,5-trichlorobenzene (TCB),[13] and 1-bromo-3,5-dichlorobenzene (DCBB).[14] Furthermore, thiophene has been considered as a potential additive because of being successfully used in the construction of organic photovoltaic materials.[15] Recently, Huang et al. used difluoronated thiophenes (FBrT) as solvent additives in mediating morphologies and achieved efficient organic solar cells, demonstrating the capability of functionalized thiophene in regulating the bulk heterojunction (BHJ) nanoscale morphology.[16] Because of its effectiveness, the solidification of thiophene must be realized to overcome the complicacy of fluorination and the liquid nature of FBrT so as to realize corresponding SAs. Unlike fluorine atoms, bromine and iodine have an enlarged atom size (F, 0.071; Br, 0.114; I, 0.132 nm) and loosened outer-sphere electrons, causing them to be easily polarized and facilitating stronger intermolecular interactions through the efficient orbital overlapping of π/p-electrons.[17] Moreover, the higher crystallinity of bromide and iodide could induce better molecular packing. These features not only can guarantee the solidification of thiophene but may also prompt the ordered crystallization of conjugated electron D/A materials, optimize the BHJ microstructure, and improve the charge-transport properties of the D/A blend film.[18]

Therefore, in this study, we designed and reported three isomeric perhalogenated thiophene derivatives, namely 3,4-dibromo-2,5-diiodothiophene (SA-T1), 2,5-dibromo-3,4-diiodothiophene (SA-T2), and 2,3-dibromo-4,5-diiodothiophene (SA-T3). With simple iodination, three SAs can be facially obtained from different dibromothiophenes. After comprehensively investigating their thermal properties and molecular interactions with respect to polymeric materials, we adopted them as SAs to tune the morphological features of typical all-polymer blends and further optimize the performance of APSCs. Specifically, compared with a PCE of ≈14% for the PM6:PY-IT-based as-cast device, these SA-treated APSCs showed satisfactory PCEs of over 17% with significantly improved short-circuit current densities (J_{sc}) and fill factors (*FF*). Notably, SA-T1-treated binary APSC showed the highest PCE of 18.3% along with enhanced thermal stability because of its better morphological features and optimal charge dynamic properties. To the best of our knowledge, our result of 18.3% PCE ranks the highest among all binary APSCs to date. When increasing the thickness of the active layer to 250 nm, the device performance can be maintained as a PCE of ≈16%, suggesting the potential of thiophene-based SA in future applications.

Results and Discussion

Figure 1a displays the chemical structures of polymer donor PM6 and polymer acceptor PY-IT, the blended films of which possess well-complementary absorptions extending to ≈900 nm and matched energy levels (Figure S1), thus providing prerequisite conditions for realizing high J_{sc} and V_{oc} parameters. From commercially available materials, we were able to synthesize three halogen-substituted thiophene derivatives in one step over a large scale (Scheme S1). As shown in Figure 1b, SA-T1, SA-T2, and SA-T3 are isomers with two types of halogen atoms (Br and I) on different substituted positions; this could affect their intrinsic properties and interactions with electron D/A materials. Furthermore, differential scanning calorimetry (DSC) measurements were conducted to determine their melting points (m.p.), which are 147, 146, and 136 °C for SA-T1, SA-T2 and SA-T3 (Figure 1c), respectively, indicating different intermolecular interactions in their solid states. The thermogravimetry analysis (TGA) results (Figure 1d) show that SA-T1 and SA-T2 were completely volatilized at the heating temperature at 150 °C, and SA-T3 volatilized up to 80% under continuous heating for 60 min; these results may be ascribed to the dehalogenation of SA-T3. The difference in the volatility and stability of the three SAs could result in variated film morphology of the host D/A blend.

In addition, Fourier-transform infrared spectra (FTIR) and UV/Vis absorption measurements were conducted to investigate whether SA-T1/SA-T2/SA-T3 would remain in the corresponding films after thermal annealing.[19] As displayed in Figure S2, the characteristic peaks of these thiophene compounds in the FTIR spectra disappear in the corresponding PM6:PY-IT blend films after thermal annealing. Similarly, the absorption profiles of SA-T1/SA-T2/SA-T3 located with 300–400 nm (Figure S3) are not observed in PM6 and PY-IT films as well as PM6:PY-IT blend films under different additive treatments (Figures 1e–1f and Figure S4). All these results imply that the thiophene derivates can be removed at a certain heating temperature, and this the basic requirement for them to be used as SAs in the tuning of the morphologies of active layers. As supportive evidence, in comparison with PM6 neat film, all SA-T1/SA-T2/SA-T3 treated PM6 films displayed ≈6 nm red-shifted absorption characteristics together with enhanced relative intensity (I_{0-0}/I_{0-1}) of 0–0 absorption peaks (Figure 1e), suggesting a more ordered interchain stacking of PM6 in the corresponding films.[20] For PY-IT films under various treatments, the absorption spectra in Figure 1f shows

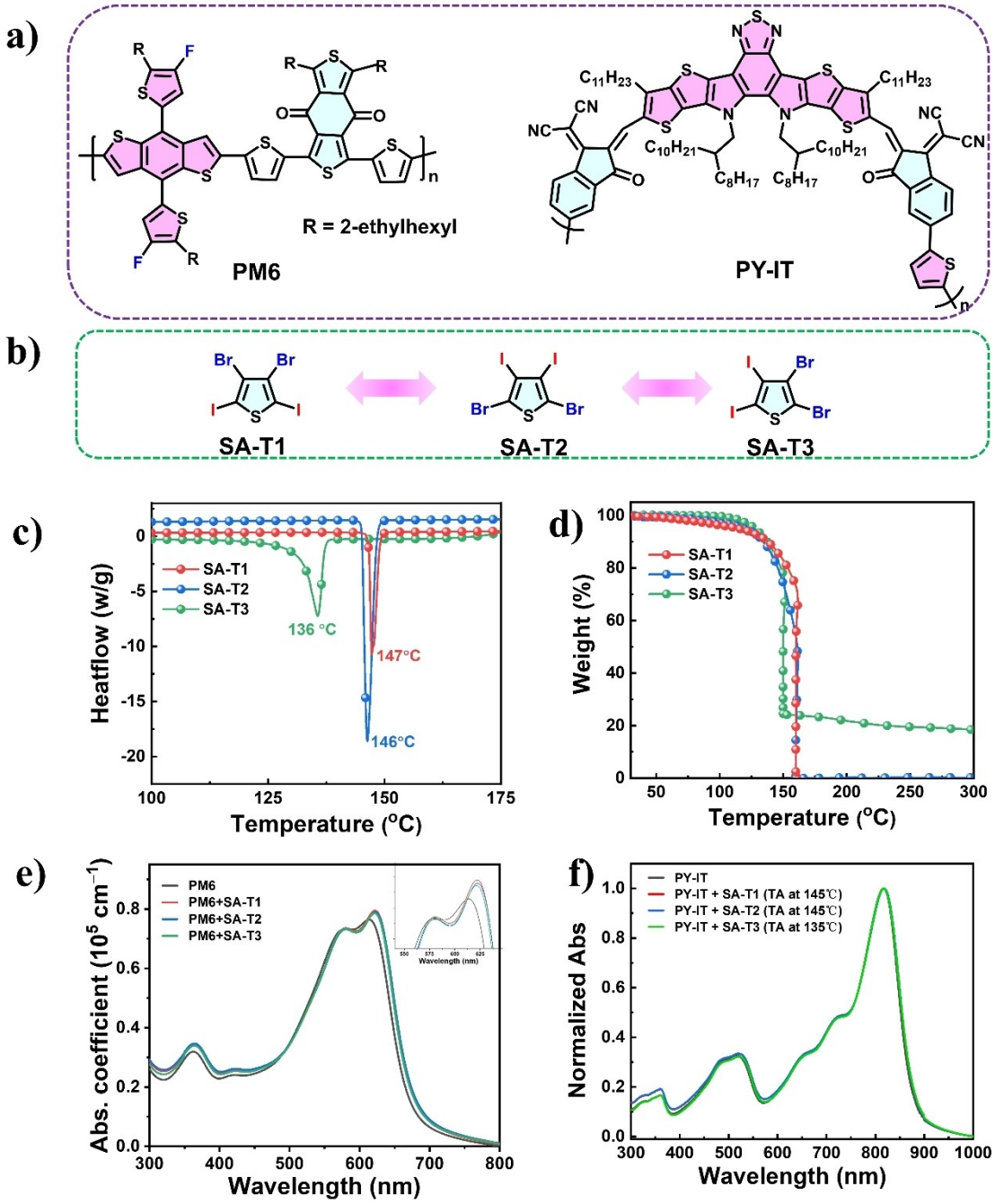

Figure 1. a) Chemical structures of polymer donor PM6 and polymer acceptor PY-IT. b) Chemical structures of SA-T1, SA-T2 and SA-T3, respectively. c) DSC and d) TGA of SA-T1, SA-T2 and SA-T3. Absorption of e) PM6 neat films, and f) PY-IT neat films with different SA treatments.

almost identical profiles with slightly red-shifted maximum absorption peaks for SA-treated films (from 816 to 818 nm). These phenomena derived from UV/Vis spectra demonstrate that the usage of SA-T1/SA-T2/SA-T3 would affect the molecular packing mode of both PM6 and PY-IT, especially the polymer-donor, PM6, as revealed through the results of grazing incidence wide-angle X-ray scattering (GIWAXS).

Figures 2a and 2b display the diffraction images of GIWAXS measurement for PM6- and PY-IT-based films, respectively, under different SA treatments. Figure S5 presents their corrsponding line-cut profiles. These results could provide insights into the molecular packings and crystallinity behaviors of films. First, the treatments of these SAs would not influence the preferred face-on molecular orientations of PM6 and PY-IT, whose (010) π–π stacking and (100) alkyl-to-alkyl stacking signals are located in the out-of-plane (OOP) and in-plane (IP) directions, respectively. Such molecular packing modes of both PM6 and PY-IT could deliver effective pathways for charge trans-

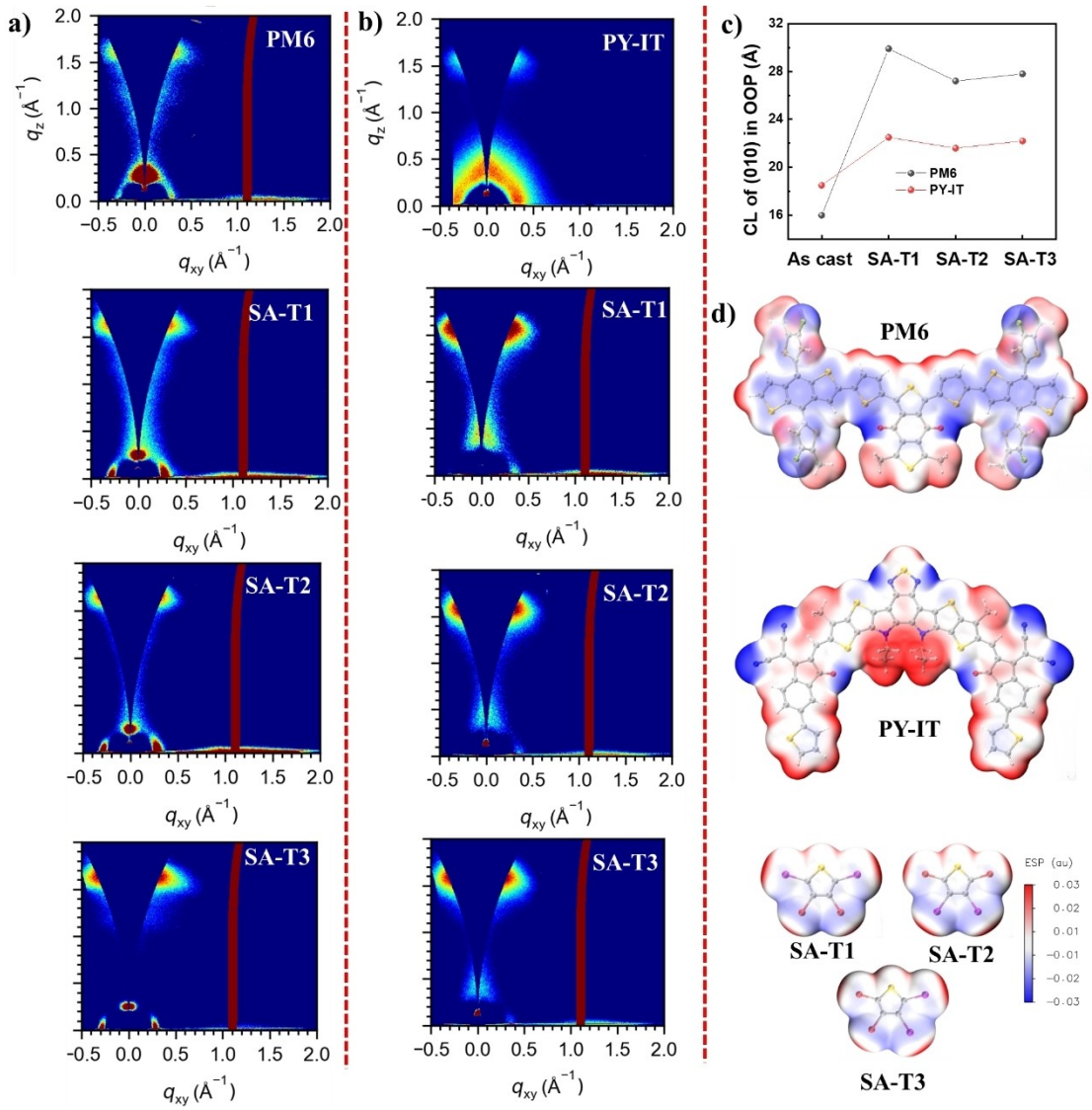

Figure 2. GIWAXS images of (a) PM6 and (b) PY-IT based films under different SAs treatment. c) Coherence lengths of (010) π–π stacking of PM6 and PY-IT based films under different SAs treatment. d) ESP mapping images of PM6 and PY-IT segments, and SA-T1/SA-T2/SA-T3, respectively.

portation in films. After the SA-based treatment, the coherence lengths (CLs) of the (010) and (100) diffractions of PM6 films are larger than those for the as-cast film (Figure 2c and Table S2). A similar tendency of CLs was observed for PY-IT films under different SA treatments. Note that after an SA-based treatment, the enhancement of CLs in the (010) π–π stackings of PM6 is more obvious than that of PY-IT (Figure 2c), suggesting that this type of SA has a better capability in tuning molecular packings of PM6. Particularly, both PM6 and PY-IT films with SA-T1-based treatment yielded the largest CLs of (010) π–π stackings, which are favorable for use in the intermolecular charge transportation, and can thus be used in realizing satisfactory *FF*s.[21] Space charge limited current (SCLC) method was used to study the charge mobility properties of PM6 and PY-IT neat films under different treatment (Figure S6). The hole mobility for the as-cast PM6 neat film is $(1.00\pm0.09)\times10^{-3}$ cm^2 V^{-1} s^{-1}, which is improved to $(1.36\pm0.05)\times10^{-3}$, $(1.28\pm0.08)\times10^{-3}$, and $(1.21\pm0.08)\times10^{-3}$ cm^2 V^{-1} s^{-1} for SA-T1, SA-T2, and SA-T3 treated films (Table S3), respetively. Meanwhile, the electron mobility for PY-IT neat film is slightly improved after SAs-based treatment. These results follow the trends of their CLs of (010) π–π stackings.

To reveal mechanisms attributable to the different molecular crystallinity behaviors of PM6 and PY-IT with SA-treatments, a theoretical approach was realized at the molecular level. The electrostatic potential (ESP) distributions of PM6 and PY-IT monomer along with SAs were approximated using the density functional theory (DFT) calculations (all the side-chains are omitted for clarity).[22] As shown in Figure 2d, the conjugated backbone of PY-IT is highly positive, whereas the negative regions are distributed mainly on the nitrogen-contained moieties (e.g., cyano group, thiadiazole) and carbonyl groups. In contrast, the backbone of PM6 is mostly negative with positively-charged

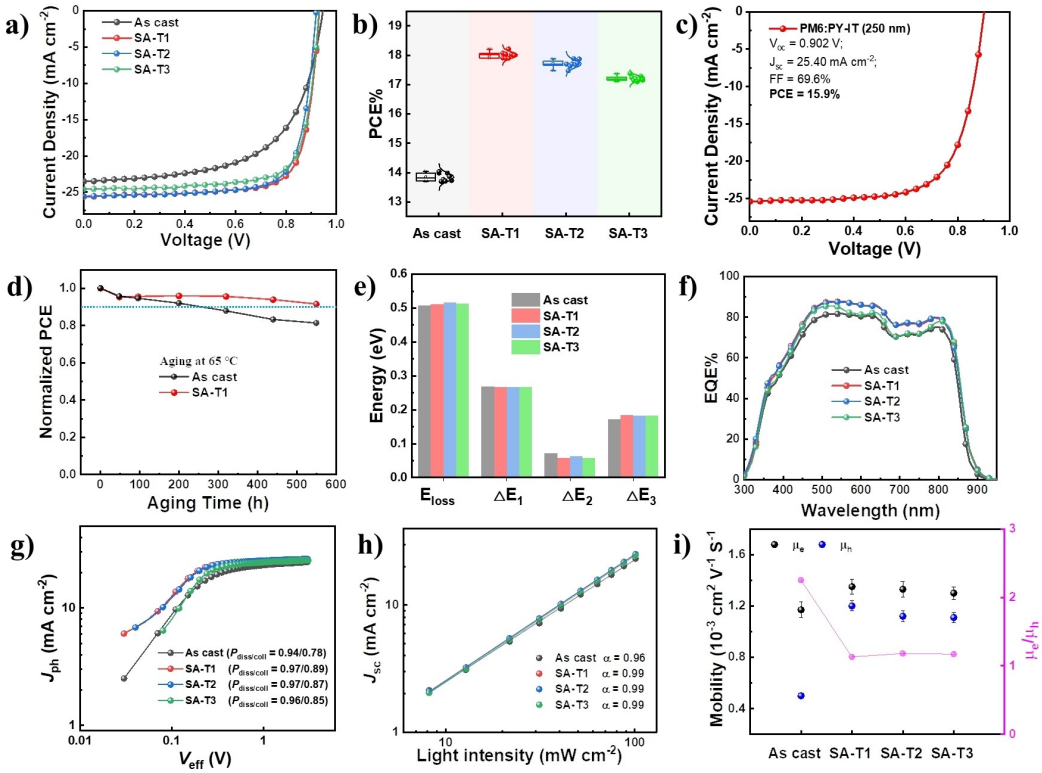

Figure 3. a) *J*–V curves and b) the distribution of top best eight devices of PM6 : PY-IT based devices under different treatments. c) *J*–V curve of APSC device with a thickness of 250 nm. d) Thermal stabilities of PM6 : PY-IT based devices without any treatment and with SA-T1 treatment. e) Energy losses of PM6 : PY-IT based devices under different treatments. f) EQE curves, g) J_{ph}–V_{eff} curves, h) J_{sc} versus light intensity, and i) hole and electron mobilities of PM6 : PY-IT based devices under different treatments.

peripheral side-chains. Furthermore, unlike most of the reported halogenated-benzene-derived SAs, the perhalogenated thiophene SAs exhibited a more positive iso-surface. Moreover, the calculated binding energy (E_B) between the perhalogenated thiophene and PM6 is higher than that between perhalogenated thiophene and PY-IT (Table S4). Based on these results, we can assume that our SAs have a stronger interaction with PM6 than PY-IT, consistent with the data obtained from UV/Vis and GIWAXS.

Based on the aforementioned results, organic solar cells with the conventional configuration of indium tin oxide (ITO)/poly (3,4-ethylenedioxythiophene)-poly (styrenesulfonate) (PEDOT : PSS)/PM6 : PY-IT/poly[[2,7-bis(2-ethylhexyl)-1,2,3,6,7,8-hexahydro-1,3,6,8-tetraoxobenzo[lmn][3,8-phenanthroline-4,9-diyl]-2,5-thiophenediyl[9,9-bis[3-(dimethylamino)propyl]-9H-fluorene-2,7-diyl]-2,5-thiophenediyl] (PNDIT-F3N)/Ag were fabricated to demonstrate the potential of these thiophene derivatives as SAs in controlling device performance of APSCs. Note that, the post thermal annealing treatment is necessary for removing the SAs from active layers. The ratios of SAs to those post treatments were carefully tuned to present their optimal devices (Table S5), with their optimal current–voltage (*J*–V) curves and PCE distributions presented in Figures 3a and 3b, respectively. In addition to the device parameters summarized in Table 1, we can conclude that the unfavorable J_{sc} of 23.25 mA cm^{-2} and *FF* of 64.1 % limit the overall

Table 1: Photovoltaic parameters of PM6 : PY-IT based devices under different treatments.

Treatments	V_{oc} (V)	J_{sc} (mA cm^{-2})	J_{sc}^{CAL} (mA cm^{-2})	FF %	PCE %
As cast	0.946	23.25	22.89	64.1	14.1 (13.8 ± 0.1)
SA-T1	0.933	25.61	24.80	76.5	18.3 (18.0 ± 0.1)
SA-T2	0.926	25.55	24.73	75.7	17.9 (17.7 ± 0.1)
SA-T3	0.932	24.57	23.82	75.9	17.4 (17.3 ± 0.1)

PCE of 14.1 % for PM6 : PY-IT-based as-cast devices. After SA-based treatment, significant improvements were observed in the J_{sc} and *FF* values for their corresponding binary devices. In addition, three SA-treated devices obtained PCEs of 17.4 %–18.3 %, attributed to the slight differences in three photovoltaic parameters, which were caused by their charge dynamics and morphological features, as discussed below. Perbromothiophene (4Br-T) and periodothiophene (4I-T) were also used as the SAs to optimize the performance of APSCs. As seen in Table S5, though PCEs over 15 % could be realized in 4Br-T and 4I-T treated devices, they are much lower than those of our developed SAs-treated devices. Notably, SA-T1-treated devices demonstrate a promising PCE of 18.3 %, which is ranked as the best among binary all APSCs to date, and is comparable to the high-performance ternary deivces (see the summary in Table S1). Furthermore, a PCE of ≈16 %

could be obtained by increasing the thickness of SA-T1-treated active layer to ≈250 nm (Figure 3c). Accordingly, a 1.32 cm^2 device prepapred by spin-coating method deliered a PCE of 15.2 % (Figure S7). Furthermore, PM6:PY-IT based flexible solar cell under SA-T1 treatment achieved a PCE of 15.1 %, which could be maintained over 90 % after bending for 1000 cycles under the bending radius of 5 mm (Figure S8).The long-term stability of OSCs has become one of the most concerned issues nowadays.[23] As depicted in Figure 3d, under continuous heating at 65 °C, the thermal stability of SA-T1-treated device is improved with a T_{90} lifetime of 550 h, which is double that of the as-cast device (T_{90} = 250 h). All these results demonstrate a possibility for the future applications of SA-T1-treated APSCs.

The decent performances of three SAs-treated devices are also closely relevant to their reasonable high open-circuit voltages (V_{oc}s) of ≈0.93 V, especially considering their narrow band gaps (E_gs) of ≈1.45 eV (Figure S9). After systematically calculating energy losses (E_{loss}) of the devices based on the Shockley–Queisser (SQ) limit theory,[24] rather similar and low E_{loss} values of approximately 0.51 eV were observed for all devices under as-cast and SAs-treating conditions (Table S6). As shown in Figure 3e, the detailed illustrations of the three parts (ΔE_1, ΔE_2 and ΔE_3) for the overall E_{loss} suggest that the usage of SAs only slightly affects the radiative and nonradiative energy losses, echoing their slightly different V_{oc} parameters. Subsequently, their different J_{sc} values derived from *J*–V curves were verified through external quantum efficiency (EQE) measurements, which integrate the J_{sc} values of 22.89, 24.80, 24.73, and 23.82 mA cm^{-2} for the as-cast, SA-T1-, SA-T2-, and SA-T3-treated devices, respectively. As shown in Figure 3f, compared with the as-cast device, SA-T1- and SA-T2-treated devices yielded obvious increments across the overall EQE response ranges, resulting in their ≈2 mA cm^{-2} enhancements in J_{sc}. Whereas, the EQE curve of the SA-T3-treated device lies in the middle of the other curves. Generally, various EQE responses support the different J_{sc} values and reflect the charge dynamic properties of the corresponding devices. Meanwhile, the thick-film device achieved an integrated J_{sc} value of 24.54 mA cm^{-2} (Figure S10), supporting its J_{sc} value derived from *J*–*V* curve.

According to previously reported methods, the exciton dissociation and charge-collection efficiencies (P_{diss} and P_{coll}) of all the devices were studied by measuring the photogenerated current density (J_{ph}) with respect to the effective voltage (V_{eff}). As depicted in Figure 3g, the P_{diss} and P_{coll} of the as-cast device were calculated to be 0.94 and 0.78, respectively, indicating the occurrences of unfavorable charge generation and collection processes, thus explaining this device's low J_{sc} and *FF* values. For SA-treated devices, higher P_{diss} and P_{coll} parameters were realized simultaneously, supporting their favorable J_{sc} and *FF* values. Note that the most efficient charge-collection behaviors are observed in SA-T1-treated device, accounting for its highest FF of 76.5 %. In addition, charge-recombination mechanisms were evaluated by establishing the relationship of current density under different light intensities (P_{in}), which follows the power-law relations of $J_{sc} \propto P_{in}^{\alpha}$. As a result, the value of α was improved from 0.96 for the as-cast device to 0.99 for the SA-treated devices (Figure 3h). Such results indicate similar but negligible bimolecular recombination, thus showing the advantage of realizing high *FF*s in all SA-treated devices.

Generally, charge-recombination and collection procedures are closely related to their abilities of charge transportation. Therefore, SCLC method was adopted by fabricating hole-only and electron-only devices to measure the hole and electron mobilities (μ_h and μ_e) in all devices (Figure S11). For the as-cast device, $\mu_h = 0.52\times10^{-3}$ $cm^2 V^{-1} s^{-1}$, which is lower than half that of $\mu_e = 1.17\times10^{-3}$ $cm^2 V^{-1} s^{-1}$. The unbalanced charge transporting in the as-cast device causes the undesired charge recombination, resulting in its low *FF* of 64.1 %. After the treatment with SAs, both hole and electron mobilities were enhanced. In particular, hole mobilities were improved to the same level of electron mobilities in all SA-treated devices. As such, compared with the as-cast device, the SAs-treated devices exhibited higher and more balanced μ_h and μ_e (Figure 3i). Moreover, the observed reduced charge recombination as well as the faster and efficient charge transportation of all SA-treated devices were assumed as the key factors for improving the J_{sc} and *FF* values.[25] All these abovementioned indicators suggest that the SA-T1-treated device demonstrated the most efficient charge collection (P_{coll} = 0.89) and charge transportation ($\mu_h = 1.20\times10^{-3}$ $cm^2 V^{-1} s^{-1}$ and $\mu_e = 1.35\times10^{-3}$ $cm^2 V^{-1} s^{-1}$), accounting for the highest values of J_{sc} and *FF* among all three SA-treated devices.

To reveal the effect of these SAs on their morphological features, which play a vital role on the charge dynamic properties, atomic force microscopy (AFM) and GIWAXS measurements were conducted for PM6:PY-IT blend films with different treatments. AFM height images of all the blend films (Figure S12) show their uniformity and smoothness with a small root-mean-square (RMS) roughness of approximately 0.80 nm, which is beneficial for forming good ohmic contact with the PNDIT-F3N layer. Additionally, compared with the as-cast PM6:PY-IT film, the SA-treated blend films yielded clearer and a more consecutive fibril network, as displayed by their AFM phase images (Figure 4a). Subsequently, the diameters of such featured nanofibrils were analyzed according to previously reported methods.[26] As shown in Figure 4c, the PM6:PY-IT as-cast film displays large nanofibrils with diameters of 23.8 ± 6.4 nm, and such unoptimized morphological features are detrimental for exciton separation as well as charge generation. It is worth noting that the diameters of nanofibrils were reduced to 16.0 ± 4.1, 17.3 ± 4.0, and 20.0 ± 5.9 nm for SA-T1-, SA-T2-, and SA-T3-treated blend films (Figure S13), respectively, which are thought to be within the distance of exciton diffusion, and thus could enable an effective charge-generation process. Besides, the miscibility of PM6 and PY-IT under different treatment was evaluated by the Flory-Huggins parameters (χ_{D-A}, Figure S14 and Table S7).[27] As the results show, the as-cast PM6 and PY-IT blend displays a χ_{D-A} of 0.27 K (K is a constant). While, after SA-treating, all PM6:PY-IT blends show reduced χ_{D-A}, suggesting better miscibility of PM6 and PY-

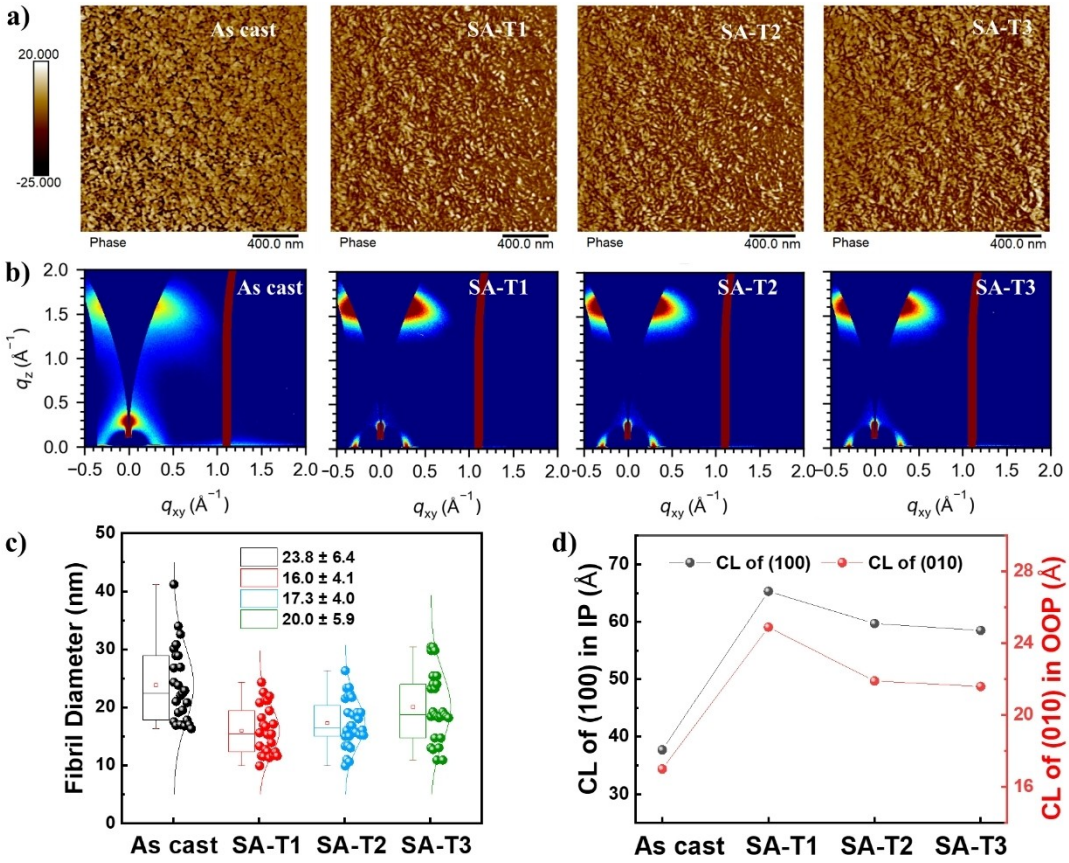

Figure 4. a) AFM images and b) GIWAXS images of PM6 : PY-IT blend films with different treatments. c) The statistical distribution of the fibril width for PM6 : PY-IT blended films under different treatments. d) Coherence lengths of (100) in IP and (010) in OOP for the corresponding GIWAXS results. Coherence lengths are calculated using the Scherer equation.

IT in the corresponding blends. Furthermore, the χ_{D-A} of SA-T1/SA-T2/SA-T3 treated blends are gradually increased from 0.12 K to 0.15 K to 0.18 K, respectively, which is an indicator of gradually reduced miscibility of PM6 and PY-IT in the blend films, contributing to their various nanofibril diameters to some extent.

Furthermore, GIWAXS results demonstrate the impact of these SAs on molecular packings and crystallinities (Figure 4b). All four blend films showed an obviously (010) π–π stacking signal along the q_z direction (IP) and (100) diffraction along the q_{xy} direction (OOP), implying that the preferred face-on molecular orientations in the PM6 : PY-IT films can be well maintained after different SA treatments.[28] Figure S15 shows the corresponding line-cuts of IP and OOP directions, and Table S8 lists the parameters. Compared to the as-cast blend film, all SA-treated films showed slightly smaller π–π stacking distances of ≈3.90 Å, indicating more condensed molecular packings between conjugated skeletons. Combined with the obviously enhanced CLs in both (010) and (100) diffraction areas after SA treatment (Figure 4d), more effective charge-transport pathways could be established in the corresponding blend films.[29] Overall, these results indicate that the treatments of SAs could reinforce molecular packing and realize suitable CLs, which is beneficial for achieving high J_{sc} and *FF* values for these SA-treated devices.[30] Among all the SA-treated devices, the SA-T1-treated blend film exhibited the largest CL of π–π stacking (24.9 Å) and alkyl-to-alkyl stacking (65.3 Å), contributing to its highest charge mobilities and thus the best device performance. Furthermore, the morphological features of the SA-T1-treated device, such as distinctive nanofibrils with diameters of 16.0 ± 4.1 nm and enhanced molecular packing, might be partially responsible for its decent thermal stability, as discussed earlier.

As a matter of fact, after spin-coating from the chloroform solutions, white granular SAs could be clearly observed on the surface of corresponding films (Figure S16). After thermal anmealing, SAs were evaporated and the surface of blend films became smooth. To gain more insight into the mechanism of SA assisted morphology formation, in situ UV/Vis absorption measurements were conducted for all the blend films under thermal annealing. The absorptions along with thermal annealing time are oberved for these PM6 : PY-IT blends (Figure 5) and the progress vary significantly. The progress of thermal annealing could be divided into three stages for each blend. For the as-cast PM6 : PY-IT film, the main abosrption peaks of PM6 and PY-IT are located at 617 and 807 nm, respectively. After these SA-based treatments, the main abosrption peak of PM6 are red-

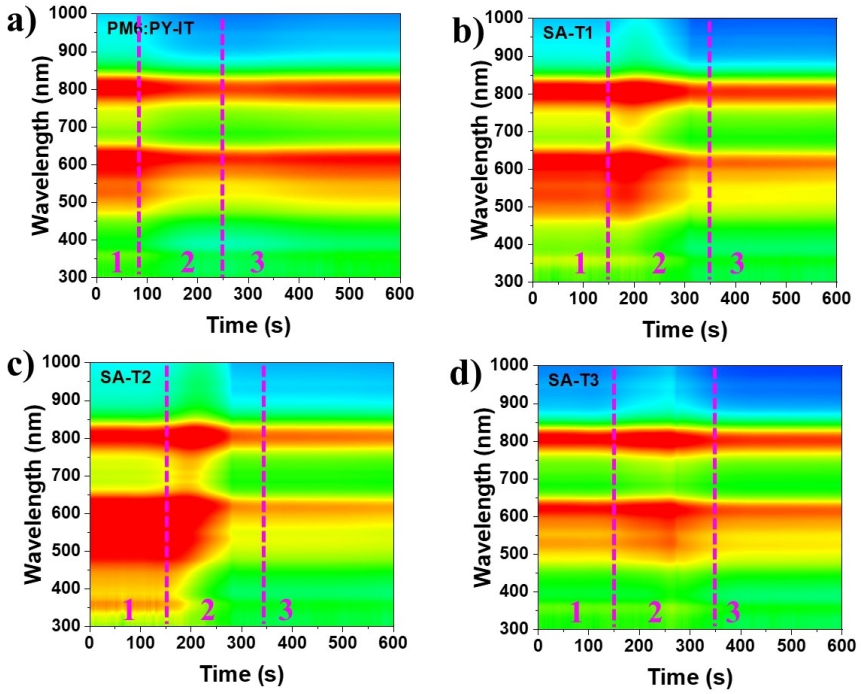

Figure 5. In situ UV/Vis absorption of PM6 : PY-IT blend film under different SA-based treatments. a) PM6 : PY-IT, b) SA-T1-treated PM6 : PY-IT, c) SA-T2-treated PM6 : PY-IT, and d) SA-T3-treated PM6 : PY-IT, respectively.

shifted to ca. 621 nm, and the absorption profile of PY-IT remain intact.

As the thermal annealing initiated, the absorbances of these blend films stay unchanged for a while (Stage 1: ca. 70 s for as-cast film, and ca. 150 s for SA-treated films). The different time of stage 1 for these blend films may be ascribed to the different heat condution process as well as the influence of the residual SAs in the blends films. After then, the absorption profiles of all blend films began to reform (Stage 2), which can be ascribed to the movement and rearrangements of polymer chains. In comparison with as-cast film, all SA-treated films displayed distinct absorption behaviour in stage 2 from ca. 150 to ca. 350 s (Figure S17). Based on observation above, it can assumed that all SAs were removed from the all-polymer blends after continous heating, leaving considerable amount of free volume in the films; meanwhile, as we discussed earlier, all SAs show strong molecualr interaction with PM6 and PY-IT. Therefore, the thermal annealing of SA-treated blend is more benefical for the rearrangements of PM6 as well as PY-IT under stage 2, contributing to their improved molecular packings and molecular crystallinities as revealed by GIWAXS tests. Finally, all blend films show a relatively stable state along with almost unchanged absorbance in stage 3. Overall, these SAs could regulate the morphological evolutions in the all-polymer blend effectively, resulting in their optimal morpholgical features.

Finally, the SA-T1 device was selected for demonstrating the universality in optimizing the performance of APSCs, in which PM6 : PY-DT, PM6 : PY-V-γ,[31] and PM6 : PYF-T-*o*[32] were adopted as active layers (Figure 6a). The *J*–V curves of as-cast and SA-T1-treated devices are depicted in Figure 6b, and device parameters are summarized in Table 2. Compared with their as-cast devices, all SA-T1-treated devices achieved significant improvements with better PCEs, such as 17.4 % for PM6 : PY-DT, 17.0 % for PM6 : PY-V-γ, and 16.1 % for PM6 : PYF-T-*o*-based APSCs. These improvements could be mainly attributed to their favorable J_{sc} and *FF* values. As shown in Figure 5c, the SA-T1 device displayed higher EQE responses, implying more efficient photoelectrical conversion processes. Generally, these results are consistent with those of PM6 : PY-IT-based devices, suggesting the success of SA-T1 in obtaining high-performance APSCs.

Conclusion

To sum up, a set of perhalogenated thiophenes was designed and served as solid additives in tuning the morpholgical

Table 2: Device parameters of PM6 : PY-DT, PM6 : PY-V-γ, and PM6 : PYF-T-*o* based all-polymer devices.

BHJ	Treatment	V_{oc} (V)	J_{sc} (mA cm^{-2})	J_{sc}^{CAL} (mA cm^{-2})	FF %	PCE %
PM6 : PY-DT	As cast	0.983	23.10	22.36	61.6	14.0
	SA-T1	0.947	24.37	23.68	75.2	17.3
PM6 : PY-V-γ	As cast	0.912	24.59	23.96	67.5	15.1
	SA-T1	0.889	25.11	24.41	76.1	17.0
PM6 : PYF-T-*o*	As cast	0.924	23.94	23.13	64.7	14.3
	SA-T1	0.873	25.88	24.95	71.3	16.1

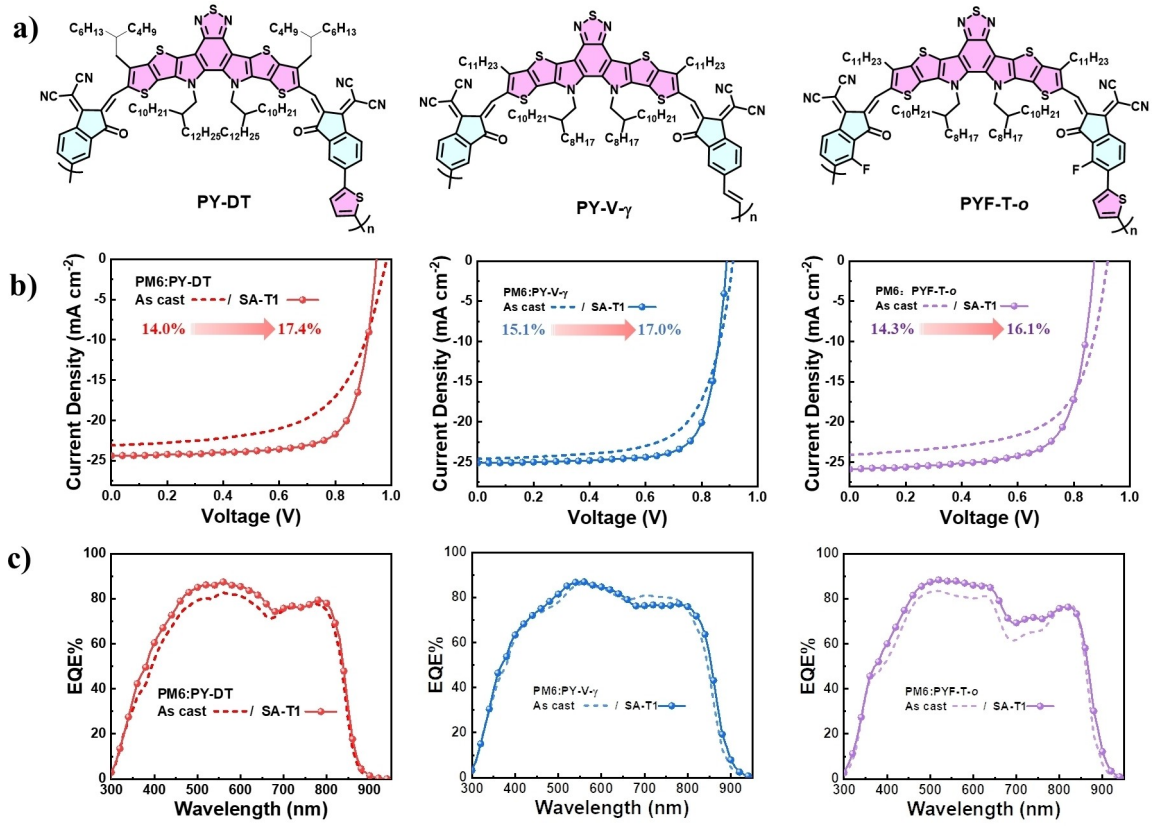

Figure 6. a Chemical structures of PY-DT, PY-V-γ, and PYF-T-*o*, respectively. b) *J*–V curves and c) EQE curves of PM6:PY-DT, PM6:PY-V-γ, and PM6:PYF-T-*o* based as-cast devices and SA-T1 treated devices, respectively.

characters of all-polymer blends. Three isomeric thiophenes (SA-T1, SA-T2, and SA-T3) are isomers with two types of halogen atoms (Br and I) on different substituted positions, resulting their variated interactions with polymer donor and polymer acceptors. As results, enhanced molecular packing and optimal nanofibers morphologies could be realized for the PM6:PY-IT blends after using these solid additives. In comparison with as-cast binary APSC, all SA-treated devices displayed suppressed charge recombinaiton and improved charge transportation beharios, contributing to their simultaneously boosted J_{sc} and *FF* values. Overall, the PCE was improved from 14.1 % for as-cast device to 17.4–18.3 % for SA-treated devices. Notably, owing to the better morphological features and optimal charge dynamic properties, SA-T1-treated binary APSC showed the highest PCE of 18.3 % along with enhanced thermal stability (T_{90} lifetime is 550 hours), ranking the highest among all binary APSCs to date. Besides, the SA-T1 shows rather good universality in optimizing the performance of APSCs, where three different all-polymer based OSCs achieved higher PCEs after SA-T1-based treatment. Our work not only highlights the importance of novel SAs in tuning the morphologies and thus improving the device performance of APSCs, but also provides a new pathways to develop SAs for APSCs.

Acknowledgements

The authors gratefully acknowledge the financial support from MoST of China (2022YFB4200400, 2019YFA0705900), NSFC (21935007, 52025033, 52303237, and 22361132530) and Natural Science Foundation of Chongqing (CSTB2023NSCQMSX0268). The authors thank Yu Chen at the Beijing Synchrotron Radiation Facility, Institute of High Energy Physics for performing GIWAXS measurements.

Conflict of Interest

The authors declare no conflict of interest.

Data Availability Statement

The data that support the findings of this study are available from the corresponding author upon reasonable request.

Keywords: All-Polymer Solar Cells · Halogenated Thiophene · High-Efficiency · Morphology · Solid Additives

[1] a) J. Liu, J. Deng, Y. Zhu, X. Geng, L. Zhang, S. Y. Jeong, D. Zhou, H. Y. Woo, D. Chen, F. Wu, L. Chen, *Adv. Mater.* **2023**,

35, 2208008; b) Z. Wang, M. Xu, Z. Li, Y. Gao, L. Yang, D. Zhang, M. Shao, *Adv. Funct. Mater.* **2021**, *31*, 2103534; c) T. Kim, J. H. Kim, T. E. Kang, C. Lee, H. Kang, M. Shin, C. Wang, B. Ma, U. Jeong, T. S. Kim, B. J. Kim, *Nat. Commun.* **2015**, *6*, 8547; d) Z. Genene, J. W. Lee, S. W. Lee, Q. Chen, Z. Tan, B. A. Abdulahi, D. Yu, T. S. Kim, B. J. Kim, E. Wang, *Adv. Mater.* **2022**, *34*, 2107361.

[2] a) Z. Liu, Q. Li, L. Fu, J. Wang, J. Ma, C. Zhang, R. Wang, *Adv. Sci.* **2023**, *10*, 2301931; b) Z. Zhang, Y. Yang, J. Yao, L. Xue, S. Chen, X. Li, W. Morrison, C. Yang, Y. Li, *Angew. Chem. Int. Ed.* **2017**, *56*, 13503–13507; c) H. Yu, M. Pan, R. Sun, I. Agunawela, J. Zhang, Y. Li, Z. Qi, H. Han, X. Zou, W. Zhou, S. Chen, J. Y. L. Lai, S. Luo, Z. Luo, D. Zhao, X. Lu, H. Ade, F. Huang, J. Min, H. Yan, *Angew. Chem. Int. Ed.* **2021**, *60*, 10137–10146; d) T. Wang, M. Chen, R. Sun, J. Min, *Chem* **2023**, *9*, 1702–1767; e) Z. Yao, X. Wan, C. Li, Y. Chen, *Acc. Mater. Res.* **2023**, *4*, 772–785.

[3] a) R. Sun, T. Wang, Q. Fan, M. Wu, X. Yang, X. Wu, Y. Yu, X. Xia, F. Cui, J. Wan, X. Lu, X. Hao, A. K. Y. Jen, E. Spiecker, J. Min, *Joule* **2023**, *7*, 221–237; b) X. Yang, R. Sun, Y. Wang, M. Chen, X. Xia, X. Lu, G. Lu, J. Min, *Adv. Mater.* **2023**, *35*, 2209350; c) P. Wu, Y. Duan, Y. Li, X. Xu, R. Li, L. Yu, Q. Peng, *Adv. Mater.* **2023**, 2306990; d) Y. Cai, C. Xie, Q. Li, C. Liu, J. Gao, M. H. Jee, J. Qiao, Y. Li, J. Song, X. Hao, H. Y. Woo, Z. Tang, Y. Zhou, C. Zhang, H. Huang, Y. Sun, *Adv. Mater.* **2023**, *35*, 2208165; e) J. Wang, Y. Cui, Y. Xu, K. Xian, P. Bi, Z. Chen, K. Zhou, L. Ma, T. Zhang, Y. Yang, Y. Zu, H. Yao, X. Hao, L. Ye, J. Hou, *Adv. Mater.* **2022**, *34*, 2205009; f) C. Zhao, R. Ma, Y. Hou, L. Zhu, X. Zou, W. Xiong, H. Hu, L. Wang, H. Yu, Y. Wang, G. Zhang, J. Yi, L. Chen, D. Wu, T. Yang, G. Li, M. Qiu, H. Yan, S. Li, G. Zhang, *Adv. Energy Mater.* **2023**, *13*, 2300904.

[4] X. Huang, Y. Sun, Z. Zhao, S. Chung, K. Cho, Z. Kan, *ACS Appl. Mater. Interfaces* **2023**, *15*, 44012–44021.

[5] a) L. Zhu, W. Zhong, C. Qiu, B. Lyu, Z. Zhou, M. Zhang, J. Song, J. Xu, J. Wang, J. Ali, W. Feng, Z. Shi, X. Gu, L. Ying, Y. Zhang, F. Liu, *Adv. Mater.* **2019**, *31*, 1902899; b) X. Xu, K. Feng, L. Yu, H. Yan, R. Li, Q. Peng, *ACS Energy Lett.* **2020**, *5*, 2434–2443.

[6] a) Z. Li, Y. Liang, X. Qian, L. Ying, Y. Cao, *Chem. Eng. J.* **2022**, *446*, 136877; b) W. Xu, X. Zhu, X. Ma, H. Zhou, X. Li, S. Y. Jeong, H. Y. Woo, Z. Zhou, Q. Sun, F. Zhang, *J. Mater. Chem. A* **2022**, *10*, 13492–13499.

[7] Y. Xie, H. S. Ryu, L. Han, Y. Cai, X. Duan, D. Wei, H. Y. Woo, Y. Sun, *Sci. China Chem.* **2021**, *64*, 2161–2168.

[8] R. Yu, H. Yao, Z. Chen, J. Xin, L. Hong, Y. Xu, Y. Zu, W. Ma, J. Hou, *Adv. Mater.* **2019**, *31*, 1900477.

[9] a) R. Yu, R. Shi, Z. He, T. Zhang, S. Li, Q. Lv, S. Sha, C. Yang, J. Hou, Z. Tan, *Angew. Chem. Int. Ed.* **2023**, *62*, e202308367; b) L. Kong, Z. Zhang, N. Zhao, Z. Cai, J. Zhang, M. Luo, X. Wang, M. Chen, W. Zhang, L. Zhang, Z. Wei, J. Chen, *Adv. Energy Mater.* **2023**, *13*, 2300763; c) G. Ding, T. Chen, M. Wang, X. Xia, C. He, X. Zheng, Y. Li, D. Zhou, X. Lu, L. Zuo, Z. Xu, H. Chen, *Nano-Micro Lett.* **2023**, *15*, 92.

[10] a) Y. Li, J. Song, Y. Dong, H. Jin, J. Xin, S. Wang, Y. Cai, L. Jiang, W. Ma, Z. Tang, Y. Sun, *Adv. Mater.* **2022**, *34*, 2110155; b) J. Song, Y. Li, Y. Cai, R. Zhang, S. Wang, J. Xin, L. Han, D. Wei, W. Ma, F. Gao, Y. Sun, *Matter* **2022**, *5*, 4047–4059.

[11] R. Zeng, L. Zhu, M. Zhang, W. Zhong, G. Zhou, J. Zhuang, T. Hao, Z. Zhou, L. Zhou, N. Hartmann, X. Xue, H. Jing, F. Han, Y. Bai, H. Wu, Z. Tang, Y. Zou, H. Zhu, C. C. Chen, Y. Zhang, F. Liu, *Nat. Commun.* **2023**, *14*, 4148.

[12] J. Fu, H. Chen, P. Huang, Q. Yu, H. Tang, S. Chen, S. Jung, K. Sun, C. Yang, S. Lu, Z. Kan, Z. Xiao, G. Li, *Nano Energy* **2021**, *84*, 105862.

[13] J. Fu, P. W. K. Fong, H. Liu, C. S. Huang, X. Lu, S. Lu, M. Abdelsamie, T. Kodalle, C. M. Sutter-Fella, Y. Yang, G. Li, *Nat. Commun.* **2023**, *14*, 1760.

[14] J. Wang, Y. Wang, P. Bi, Z. Chen, J. Qiao, J. Li, W. Wang, Z. Zheng, S. Zhang, X. Hao, J. Hou, *Adv. Mater.* **2023**, *35*, 2301583.

[15] a) Z. Li, K. Jiang, G. Yang, J. Y. L. Lai, T. Ma, J. Zhao, W. Ma, H. Yan, *Nat. Commun.* **2016**, *7*, 13094; b) X. Guo, A. Facchetti, T. J. Marks, *Chem. Rev.* **2014**, *114*, 8943–9021; c) X. Wan, C. Li, M. Zhang, Y. Chen, *Chem. Soc. Rev.* **2020**, *49*, 2828–2842.

[16] L. Guo, Q. Li, J. Ren, Y. Xu, J. Zhang, K. Zhang, Y. Cai, S. Liu, F. Huang, *Energy Environ. Sci.* **2022**, *15*, 5137–5148.

[17] H. Chen, X. Cao, P. Wang, F. Huang, Y. Zhang, H. Liang, X. Bi, T. He, W. Feng, Y. Guo, Z. Ma, G. Long, Z. Yao, B. Kan, C. Li, X. Wan, Y. Chen, *J. Mater. Chem. A* **2023**, *11*, 25368–25376.

[18] T. Duan, W. Feng, Y. Li, Z. Li, Z. Zhang, H. Liang, H. Chen, C. Zhong, S. Jeong, C. Yang, S. Chen, S. Lu, O. A. Rakitin, C. Li, X. Wan, B. Kan, Y. Chen, *Angew. Chem. Int. Ed.* **2023**, *62*, e202308832.

[19] a) L. Zhong, S. Jeong, S. Lee, T. L. H. Mai, J. Park, J. Park, W. Kim, C. Yang, *Chem. Commun.* **2023**, *59*, 12108–12111; b) L. Zhong, Z. Sun, S. Lee, S. Jeong, S. Jung, Y. Cho, J. Park, J. Park, S. Yoon, C. Yang, *Adv. Funct. Mater.* **2023**, *33*, 2305450.

[20] L. Zhong, S. H. Kang, J. Oh, S. Jung, Y. Cho, G. Park, S. Lee, S. J. Yoon, H. Park, C. Yang, *Adv. Funct. Mater.* **2022**, *32*, 2201080.

[21] H. Chen, B. Kan, P. Wang, W. Feng, L. Li, S. Zhang, T. Chen, Y. Yang, T. Duan, Z. Yao, C. Li, X. Wan, Y. Chen, *Angew. Chem. Int. Ed.* **2023**, *62*, e202307962.

[22] a) Y. Cui, P. Zhu, X. Liao, Y. Chen, *J. Mater. Chem. C* **2020**, *8*, 15920–15939; b) V. B. R. Pedersen, S. K. Pedersen, Z. Jin, N. Kofod, B. W. Laursen, G. V. Baryshnikov, C. Nuckolls, M. Pittelkow, *Angew. Chem. Int. Ed.* **2022**, *61*, e202212293.

[23] a) C. Sun, J. W. Lee, Z. Tan, T. N. L. Phan, D. Han, H. G. Lee, S. Lee, S. K. Kwon, B. J. Kim, Y. H. Kim, *Adv. Energy Mater.* **2023**, *13*, 2301283; b) B. Li, Q. Zhang, S. Li, X. Yang, F. Yang, Y. Kong, Y. Li, Z. Wu, W. Zhang, Q. Zhao, Y. Zhang, H. Young Woo, J. Yuan, W. Ma, *Chem. Eng. J.* **2022**, *438*, 135543; c) H. Yin, C. Yan, H. Hu, J. K. W. Ho, X. Zhan, G. Li, S. K. So, *Mater. Sci. Eng. R* **2020**, *140*, 100542.

[24] a) H. Chen, Y. Zou, H. Liang, T. He, X. Xu, Y. Zhang, Z. Ma, J. Wang, M. Zhang, Q. Li, C. Li, G. Long, X. Wan, Z. Yao, Y. Chen, *Sci. China Chem.* **2022**, *65*, 1362–1373; b) A. J. Gillett, A. Privitera, R. Dilmurat, A. Karki, D. Qian, A. Pershin, G. Londi, W. K. Myers, J. Lee, J. Yuan, S. J. Ko, M. K. Riede, F. Gao, G. C. Bazan, A. Rao, T. Q. Nguyen, D. Beljonne, R. H. Friend, *Nature* **2021**, *597*, 666–671.

[25] a) B. Liu, H. Sun, J.-W. Lee, Z. Jiang, J. Qiao, J. Wang, J. Yang, K. Feng, Q. Liao, M. An, B. Li, D. Han, B. Xu, H. Lian, L. Niu, B. J. Kim, X. Guo, *Nat. Commun.* **2023**, *14*, 967; b) D. Bartesaghi, C. Perez Idel, J. Kniepert, S. Roland, M. Turbiez, D. Neher, L. J. Koster, *Nat. Commun.* **2015**, *6*, 7083.

[26] a) H. Chen, Z. Zhang, P. Wang, Y. Zhang, K. Ma, Y. Lin, T. Duan, T. He, Z. Ma, G. Long, C. Li, B. Kan, Z. Yao, X. Wan, Y. Chen, *Energy Environ. Sci.* **2023**, *16*, 1773–1782; b) L. Zhu, M. Zhang, J. Xu, C. Li, J. Yan, G. Zhou, W. Zhong, T. Hao, J. Song, X. Xue, Z. Zhou, R. Zeng, H. Zhu, C. C. Chen, R. C. I. MacKenzie, Y. Zou, J. Nelson, Y. Zhang, Y. Sun, F. Liu, *Nat. Mater.* **2022**, *21*, 656–663.

[27] a) T. Wang, J.-L. Brédas, *J. Am. Chem. Soc.* **2021**, *143*, 1822–1835; b) H. Ma, Z. Sun, M. Jeong, S. Yang, S. Jeong, S. Lee, Y. Cho, J. Park, J. Park, C. Yang, *Chem. Eng. J.* **2023**, *474*, 145531.

[28] A. Hexemer, W. Bras, J. Glossinger, E. Schaible, E. Gann, R. Kirian, A. MacDowell, M. Church, B. Rude, H. Padmore, *J. Phys. Conf. Ser.* **2010**, *247*, 012007.
[29] D. Hu, H. Tang, S. Karuthedath, Q. Chen, S. Chen, J. I. Khan, H. Liu, Q. Yang, J. Gorenflot, C. E. Petoukhoff, T. Duan, X. Lu, F. Laquai, S. Lu, *Adv. Funct. Mater.* **2022**, *33*, 2211873.
[30] Z. Li, Z. Zhang, H. Chen, Y. Zhang, Y. Q. Q. Yi, Z. Liang, B. Zhao, M. Li, C. Li, Z. Yao, X. Wan, B. Kan, Y. Chen, *Adv. Energy Mater.* **2023**, *13*, 2300301.
[31] a) H. Yu, Y. Wang, H. K. Kim, X. Wu, Y. Li, Z. Yao, M. Pan, X. Zou, J. Zhang, S. Chen, D. Zhao, F. Huang, X. Lu, Z. Zhu, H. Yan, *Adv. Mater.* **2022**, *34*, 2200361; b) H. Yu, Y. Wang, X. Zou, J. Yin, X. Shi, Y. Li, H. Zhao, L. Wang, H. M. Ng, B. Zou, X. Lu, K. S. Wong, W. Ma, Z. Zhu, H. Yan, S. Chen, *Nat. Commun.* **2023**, *14*, 2323.
[32] a) Z. Liu, X. Ma, W. Xu, S. Zhang, C. Xu, S. Young Jeong, H. Young Woo, Z. Zhou, F. Zhang, *Chem. Eng. J.* **2022**, *450*, 138146; b) C. Zhao, J. Yi, L. Wang, G. Lu, H. Huang, H. K. Kim, H. Yu, C. Xie, P. You, G. Lu, M. Qiu, H. Yan, S. Li, G. Zhang, *Nano Energy* **2022**, *104*, 107872.

Manuscript received: November 3, 2023
Accepted manuscript online: January 3, 2024
Version of record online: ■■, ■■

Research Articles

Solar Cells

W. Feng., T. Chen, Y. Li, T. Duan,* X. Jiang, C. Zhong, Y. Zhang, J. Yu, G. Lu, X. Wan, B. Kan,* Y. Chen* _____ e202316698

Binary All-polymer Solar Cells with a Perhalogenated-Thiophene-Based Solid Additive Surpass 18% Efficiency

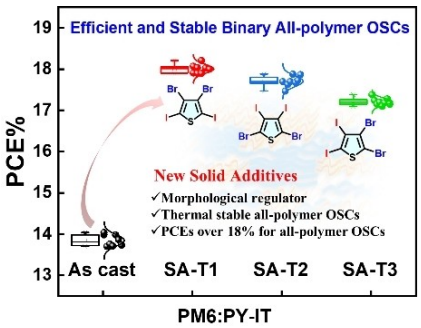

Three isomeric perhalogenated thiophenes were reported as solid additives to optimize the morphological characters of all-polymer organic solar cells (APSCs). Among them, power conversion efficiency over 18% and long-term thermal stability (T_{90} lifetime is 550 hours) were realized for SA-T1-treated binary APSC, providing a possibility for obtaining high-performance APSCs.